Reports

Magnetic Properties of Hydrothermally Recrystallized Magnetite Crystals

FRANZ HEIDER, DAVID J. DUNLOP, NAOJI SUGIURA*

The discrepancy between the magnetic hysteresis properties of magnetite crystals that are precipitated from solution (<0.3 micrometer) and of crushed sifted grains (>0.3 micrometer) is not an inherent property of magnetite but is caused by the highly stressed state of crushed material and by adhering finer fragments. The size trends of magnetic properties exhibited by submicrometer-size precipitated grains continue in the size range from 1 micrometer to 1 millimeter in a set of hydrothermally recrystallized magnetite crystals. Coercive forces of these narrowly sized crystals follow a power law over a wide size range (0.1 micrometer to 1 millimeter) as predicted by theory. Dislocation etch pits show similar dislocation densities for hydrothermally grown (3×10^{10} meter^{-2}) and natural (1×10^{10} meter^{-2}) magnetite crystals. Hysteresis parameters of hydrothermally grown crystals are similar to those of natural crystals but are about one-fifth of those for crushed grains.

AN UNDERSTANDING OF THE MAGNETIC remanence mechanisms in magnetite crystals is vital to paleomagnetists, who investigate changes in the magnetic field of the earth over millions of years as recorded by iron-titanium oxides in rocks. Applied physicists and metallurgists are concerned with coercivity mechanisms in metals, intermetallic compounds, and metal oxides in the development of better permanent magnets and magnetic recording media. Because magnetite crystals that are precipitated in solution are not easily grown to sizes greater than 1 μm, crushed materials have until now been used in studies of the size-dependent magnetic properties of magnetite grains larger than 0.3 μm in diameter (*1–5*). These crushed, irregular-shaped particles have magnetic properties that are incompatible with those of grown crystals of submicrometer size (*6, 7*).

We grew magnetite crystals of discrete size fractions in the range from 0.8 μm to 1 mm by recrystallizing 0.5-μm magnetite seed crystals hydrothermally at temperatures T between 400° and 800°C with HI and NH_4Cl solutions as mineralizers. In the only previous application of hydrothermal recrystallization to rock magnetism that we know of, Pucher (*8*) produced magnetite crystals with a wide distribution of grain sizes within one sample (0.2 to 3 μm). Our crystals are relatively well sized with standard deviations that ranged from 14 to 49% of the mean diameter. In some cases the size distributions could be improved by sieving. Details of the method are given elsewhere (*9*).

The first aim of our research was to test whether the size-dependent trends in the hysteresis properties of hydrothermally grown magnetite crystals of multidomain (MD) size continue smoothly the trends that were seen in precipitated crystals just above single-domain (SD) size (*6, 7*). The discrepancy between the theoretically calculated coercive forces H_c (*10, 11*) and the experimentally observed H_c values of crushed particles (*1–5*) can be reconciled by studying hydrothermally grown crystals. Our second aim was to grow synthetic crystals of well-defined sizes that are good analogues to naturally occurring primary magnetites. Our estimates of dislocation density from etch pits for natural magnetite single crystals and for our hydrothermally grown crystals give similar values.

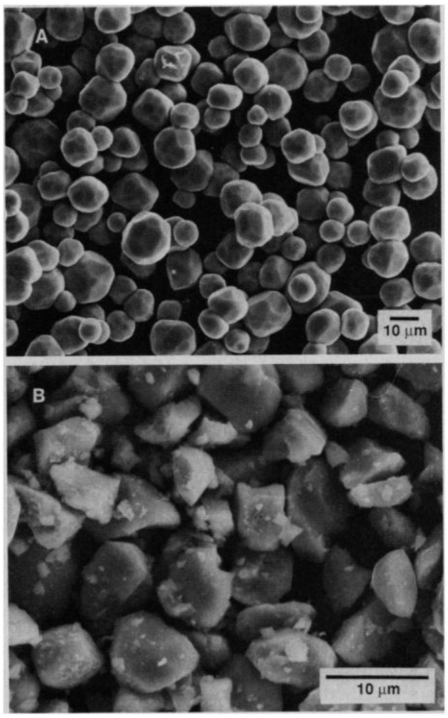

Fig. 1. Scanning electron micrographs of (**A**) hydrothermally grown euhedral magnetite crystals ($\bar{d}$ = 11.7 μm) of narrow size distribution and (**B**) irregularly shaped crushed crystals after sifting (between 3- and 7-μm sieves) and best possible cleaning from small adhering fragments.

The recrystallized magnetites are euhedral crystals whose shapes are combinations of rhombic dodecahedron, octahedron, and cube (Fig. 1A). The average diameter $\bar{d}$ and the standard deviation about $\bar{d}$ were determined by measuring the dimensions of each of about 300 crystals in scanning electron micrographs as in Fig. 1A. For comparison with hydrothermally grown samples, we ground crystals, separated them into size fractions with high-precision sieves, and removed as many adhering small particles as possible with an ultrasonic bath. This procedure yielded irregular fragments with a bimodal size distribution (Fig. 1B). The larger particles, which passed through a 7-μm sieve but were retained on a 3-μm sieve, were contaminated by magnetostatically adhering small grains. The hydrothermal magnetite crystals were free of such small particle contamination.

The near-saturation (magnetic field strength $H \leq 1$ T) hysteresis properties of hydrothermal samples with $\bar{d} < 50$ μm were measured on a vibrating sample magnetometer (VSM). Hysteresis parameters of hydrothermal crystals larger than 50 μm were measured with a magnetometer that used a superconducting quantum interference device (SQUID) in a shielded room ($H < 50$ nT), where stable reverse fields were applied with Helmholtz coils. For the two natural crystals, saturation remanence M_{rs} was measured with a spinner magnetometer and H_c was obtained by extrapolation of the descending hysteresis loop from M_{rs} to the negative H-axis. The synthetic samples contained approximately 1% magnetite by weight that was dispersed in an alumina matrix ($d \leq 0.3$ μm). Measurements for magnetite larger than 500 μm were made on single crystals.

The room-temperature coercive forces and reduced saturation remanences M_{rs}/M_s (M_s is saturation magnetization) are plotted bilogarithmically as a function of grain size in Fig. 2. There is an offset in both H_c and

---

F. Heider and D. J. Dunlop, Geophysics Laboratory, Department of Physics, University of Toronto, Toronto, Ontario M5S 1A7, Canada.
N. Sugiura, Earth and Planetary Science Laboratory, Erindale College, University of Toronto, Mississauga, Ontario L5L 1C6, Canada.

---

*Current address: Geophysical Institute, Faculty of Science, Tokyo University, Tokyo, Japan.

M_{rs}/M_s data between the size trends for crystals precipitated from solution (*6, 7*) and grains that were ground (*1–5*). We show the data of Day *et al.* (*3*) as a representative example of hysteresis data of crushed grains. The hysteresis data for our hydrothermally grown magnetite crystals, however, continue the size dependences for H_c and M_{rs}/M_s that were seen in submicrometer precipitated crystals over three decades of grain diameters, up to 1 mm (Fig. 2).

Initial susceptibility χ_0 (measured on an ac bridge) for the hydrothermally grown crystals was higher than for crushed material. For example, the 12-μm hydrothermal magnetite sample has $\chi_0 = 4.5$ and a coercivity ratio of $H_{cr}/H_c = 25$ (where H_{cr} is remanence coercivity). These values are 1.6 and 5 times, respectively, the literature values for crushed material nominally of this size. An initial susceptibility of 4.5 corresponds to a demagnetizing factor N of 0.22, if we assume a high intrinsic susceptibility. An N value of 0.22 has been calculated for a four-domain cubic grain (*12*). This prediction of four domains agrees with the few domains generally observed by the Bitter method in 10-μm size crystals. Results of the domain structure observations will be published elsewhere (*13*).

The coercive forces of hydrothermally recrystallized magnetite crystals are one-fourth to one-tenth the values reported for crushed grains. The dashed line in Fig. 2A indicates a power-law size dependence of H_c, as $H_c \propto d^{-0.57 \pm 0.06}$, for precipitated and hydrothermally grown magnetites. Our results do not agree with the recently reported hysteresis properties of magnetite particles produced by the glass-ceramic method (*14*), which do not follow a d^{-n} law. A power-law size dependence of coercive force was postulated in a theoretical model that considered the interaction of magnetic domain walls with dislocations (*10*). Power-law size dependences of H_c without offsets in the MD range have also been found for iron and cobalt (*15*). The reduced saturation remanence (Fig. 2B) shows a similar size dependence, as $M_{rs}/M_s \propto d^{-0.64 \pm 0.06}$. The uncertainties for the two exponents were determined by fitting lines with maximum and minimum slopes to Fig. 2, A and B.

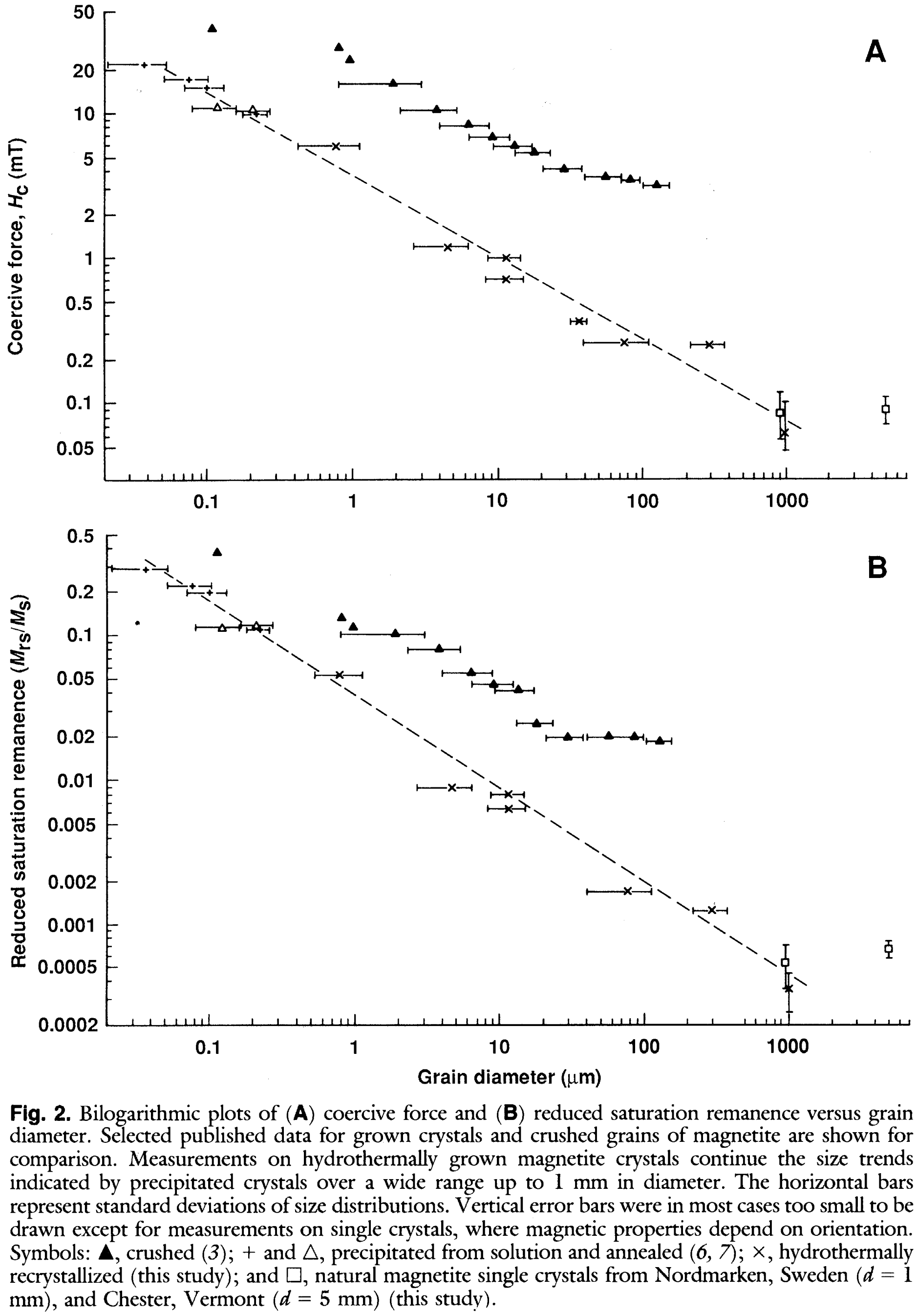

Fig. 2. Bilogarithmic plots of (**A**) coercive force and (**B**) reduced saturation remanence versus grain diameter. Selected published data for grown crystals and crushed grains of magnetite are shown for comparison. Measurements on hydrothermally grown magnetite crystals continue the size trends indicated by precipitated crystals over a wide range up to 1 mm in diameter. The horizontal bars represent standard deviations of size distributions. Vertical error bars were in most cases too small to be drawn except for measurements on single crystals, where magnetic properties depend on orientation. Symbols: ▲, crushed (*3*); + and △, precipitated from solution and annealed (*6, 7*); ×, hydrothermally recrystallized (this study); and □, natural magnetite single crystals from Nordmarken, Sweden (d = 1 mm), and Chester, Vermont (d = 5 mm) (this study).

The trends for H_c and M_{rs}/M_s with particle size for hydrothermal magnetites do not "flatten out" with increasing d as they do for crushed grains (Fig. 2). Van Oosterhout and Klomp (*16*) attributed the size dependence of H_c in magnetite to different amounts of stress caused by differential grinding. This mechanism is not relevant in hydrothermally grown crystals. The grain-size dependence of H_c and M_{rs}/M_s over 4½ decades of d, as seen in Fig. 2, is an intrinsic property of grown magnetite crystals.

The largest crystal grown hydrothermally was a 1-mm single crystal, whose coercive force is about equal to the field intensity of the earth. The coercive force of this ellipsoidal crystal (axial ratio 1:2) was lowest (0.045 mT) along the long axis and highest (0.08 mT) along the short axis as a result of the different internal demagnetizing fields. For the same reason susceptibility was highest along the long axis.

Our measurements on hydrothermally grown magnetite crystals are in good agreement with those on naturally occurring crystals. The H_c and M_{rs}/M_s values for a 1-mm single crystal of magnetite from Nordmarken, Sweden, coincide with measurements on a hydrothermally recrystallized single crystal of the same size (Fig. 2). We also investigated properties of a 5-mm magnetite octahedron from a chlorite schist in Chester, Vermont. It has slightly higher H_c and M_{rs}/M_s values than expected from the size trends in hydrothermal crystals (Fig. 2).

The similarity in hysteresis properties of natural and hydrothermal crystals prompted a comparison of their dislocation densities. A transmission electron microscope (TEM) with a tilting stage was used in studies of submicrometer-sized hydrothermal crystals; one or two dislocations were present in about 10% of the grains but no dislocations occurred in most crystals. Etching the Vermont and >30 μm hydrothermal crystals for

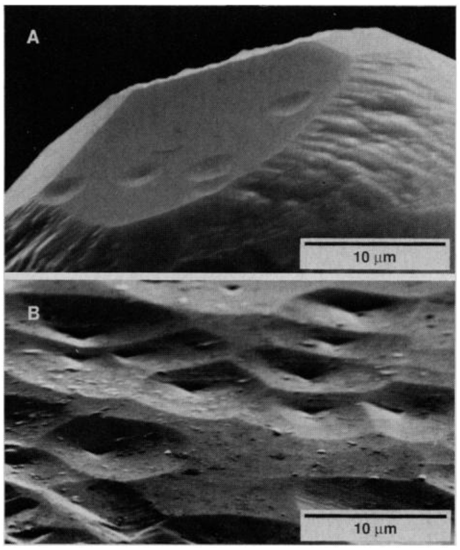

Fig. 3. Scanning electron micrographs of dislocation etch pits after etching with HCl (*18*). (**A**) Hydrothermally recrystallized magnetite ($\rho = 3 \times 10^{10}$ m^{-2}). (**B**) Natural magnetite octahedron from Chester, Vermont ($\rho = 1 \times 10^{10}$ m^{-2}). The etch pits have triangular shape as expected for {111} faces of magnetite.

10 seconds with concentrated HCl produced triangular etch pits on {111} faces. We assumed a one-to-one correspondence between such etch pits and dislocations, as is established for many materials (*17*), and determined dislocation densities ρ from etch pit counts on scanning electron micrographs. The dislocation densities are $(2.9 \pm 1.7) \times 10^{10}$ m^{-2} and $(1.0 \pm 0.8) \times 10^{10}$ m^{-2} (*18*) for the hydrothermal (Fig. 3A) and Vermont (Fig. 3B) magnetite crystals. These values are in good agreement with the value of 5×10^{10} m^{-2} found for natural titanomagnetites by Soffel (*11*) and with values of $\leq 10^{10}$ m^{-2} in undeformed grown nonmetallic crystals (*17*).

We used the theoretical model of Stacey and Wise (*10*) to calculate a value for H_c of 0.67 mT for a 12-μm grain with a single dislocation. To explain our experimental H_c values of 0.7 and 1.0 mT in the two 12-μm samples (Fig. 2A), we require $\rho = 10^{10}$ m^{-2}. This value coincides with the lower end of our measured range of values for ρ. Soffel (*11*) obtained $H_c = 0.15$ mT for the interaction of a domain wall with a single dislocation in a 10-μm cube. A dislocation density of 6×10^{10} m^{-2} is needed in this model to obtain the same value of H_c measured for our 12-μm magnetite. A certain contribution to H_c from spherical inclusions is possible, but the few small voids we observed in polished thin sections can account for only a small part of H_c (*11*). Both theoretical models can explain coercive forces in hydrothermal crystals with dislocation densities near the ones we observed. To explain H_c values typically observed in crushed grains would require $\rho \approx 10^{13}$ m^{-2}, which is several orders of magnitude greater than the value observed for natural and hydrothermally grown magnetite crystals.

High-temperature hysteresis measurements were made with the VSM to further investigate the mechanism of coercivity. Pure hydrothermal magnetite ($\bar{d} = 12$ μm) was encapsulated in quartz under vacuum. Measured values of H_c, M_{rs}, and M_s as a function of temperature are shown in Fig. 4. The Curie point was $T_c = 576° \pm 5°$C (*18*). Room-temperature hysteresis properties were remeasured after the heating experiment and were found to be unchanged.

Both H_c and M_{rs} decrease in similar ways with increasing T (Fig. 4). This behavior is consistent with an MD wall-pinning model. If H_c is magnetostrictively controlled, as a result of the interaction of domain walls (DWs) with dislocations, one expects the dependence $H_c \propto \lambda_{111}/M_s$ (*19*) (where λ_{111} is the magnetostriction constant). This dependence, which was calculated with the data of Klapel and Shive (*19*) for λ_{111}, is sketched in Fig. 4; it varies approximately as M_s^2.

The effect of nonferromagnetic inclusions on DW motion depends on the size δ_i of the inclusion. For inclusions much smaller than the DW thickness δ_w there are two sources for H_c (*11*):

1) H_c due to a reduction of DW volume:

$$H_{c,vol} \propto \frac{\gamma_w}{\delta_w^2 M_s} \propto \frac{\sqrt{A K}}{(A/K)\, M_s} \propto M_s^{10}$$

where γ_w is specific DW energy, K is the magnetocrystalline anisotropy constant, which varies as $K(T) \propto M_s^8$ (*20*), and A is the exchange constant. The value for A in magnetite was calculated by Döring from spinwave dispersion data as $A = 1.1 \times 10^{-11}$ J m^{-1} (*21*). The temperature dependence of A in magnetite can be obtained from inelastic neutron scattering at temperatures up to 570°C; A varies approximately as M_s^2 (*21*).

2) H_c due to the disperse field of the inclusion acting on the DW:

$$H_{c,disp} \propto \frac{M_s}{(A/K)^{\frac{3}{2}}} \propto M_s^{10}$$

For large inclusions ($\delta_i \geq \delta_w$) the T dependence of H_c is predicted to be (*11*):

$$H_{c,disp} \propto \frac{\sqrt{A K}}{M_s} \propto M_s^4$$

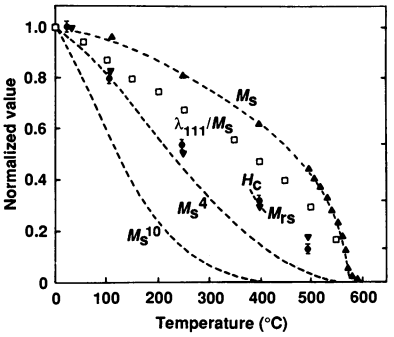

Fig. 4. Temperature dependence of normalized saturation magnetization M_s (▲, this study), reduced magnetostriction constant λ_{111}/M_s [□, (*19*)], coercive force H_c (●, this study), and saturation remanence M_{rs} (▼, this study). H_c for inclusions larger than DW varies as M_s^4, whereas H_c for inclusions smaller than DW varies as M_s^{10}.

The rapid initial decrease of H_c and M_{rs} for $T < 200°$C (Fig. 4) probably indicates partial control by large inclusions ($H_c \propto M_s^4$), whereas the slower decrease of H_c and M_{rs} at higher T suggests partial control by dislocations. The overall trend of our H_c and M_{rs} data is approximately as $M_s^{2.5}$. It is therefore closer to a dislocation-controlled trend, in agreement with the trend of low-temperature H_c data for natural magnetite (*22*).

The previous understanding of hysteresis properties was that H_c and M_{rs}/M_s decrease slowly with increasing d above approximately 25 μm (*3*). This behavior was thought to be characteristic of large "true" MD grains. The steeper size trends of H_c and M_{rs}/M_s below 25 μm were conjectured to be due to either a different degree of ordering of dislocations or a combination of magnetization curling and buckling (*3, 6*). We find no evidence for two power-law segments in the hysteresis properties of hydrothermal magnetite. A simple power law dependence as $d^{-0.6}$ can account for hysteresis properties of grown crystals from 0.1 μm to 1 mm, which suggests the same physical mechanism of coercivity (dislocations) over this wide MD range.

REFERENCES AND NOTES

1. L. G. Parry, *Philos. Mag.* **11**, 303 (1965).
2. A. A. Rahman, A. D. Duncan, L. G. Parry, *Riv. Ital. Geofis.* **22**, 259 (1973).
3. R. Day, M. Fuller, V. A. Schmidt, *Phys. Earth Planet. Inter.* **13**, 260 (1977).
4. P. Dankers and N. Sugiura, *Earth Planet. Sci. Lett.* **56**, 422 (1981).
5. R. L. Hartstra, *Geophys. J. R. Astron. Soc.* **71**, 477 (1982).
6. D. J. Dunlop, *J. Geophys. Res.* **91**, 9569 (1986).
7. S. Levi and R. T. Merrill, *ibid.* **83**, 309 (1978).
8. R. Pucher, *Earth Planet. Sci. Lett.* **6**, 107 (1969).
9. F. Heider and L. T. Bryndzia, *J. Cryst. Growth*, in press.
10. F. D. Stacey, *Adv. Phys.* **12**, 45 (1963); ______ and K. N. Wise, *Aust. J. Phys.* **20**, 507 (1967).
11. H. Soffel, *Z. Geophys.* **36**, 113 (1970).
12. D. J. Dunlop, *Geophys. Res. Lett.* **10**, 79 (1983).
13. F. Heider and S. L. Halgedahl, unpublished results.
14. H.-U. Worm and H. Markert, *Phys. Earth Planet. Inter.*, in press.
15. W. H. Meiklejohn, *Rev. Modern Phys.* **25**, 302 (1953).
16. G. W. Van Oosterhout and C. J. Klomp, *Appl. Sci. Res.* **9**, 288 (1962).
17. F. L. Vogel, W. G. Pfann, H. E. Corey, E. E. Thomas, *Phys. Rev.* **90**, 489 (1953); J. J. Gilman,

W. G. Johnston, G. W. Sears, *J. Appl. Phys.* **29**, 747 (1958); W. G. Johnston, in *Progress in Ceramic Science*, J. E. Burke, Ed. (Pergamon, Oxford, 1962), vol. 2, p. 1.
18. The mean dislocation densities and standard deviations for the Vermont and hydrothermal magnetite were determined from 10 and 15 scanning electron micrographs, respectively. The error limits on the T_c determination result from errors in graphical extrapolation of $M_s(T)$ (Fig. 4) to the T-axis (±4°C) and from uncertainty in the temperature calibration of the thermocouple (±3°C).
19. G. D. Klapel and P. N. Shive, *J. Geophys. Res.* **79**, 2629 (1974).
20. E. J. Fletcher, thesis, University of Newcastle upon Tyne, England (1975).
21. W. Döring, in *Handbuch der Physik*, S. Flügge, Ed. (Springer-Verlag, Berlin, 1966), vol. 18/2, p. 378; B. N. Brockhouse and H. Watanabe, in *Inelastic Scattering of Neutrons in Solids and Liquids* (International Atomic Energy Agency, Vienna, 1963), vol. 2, p. 297; M. F. Collins and D. H. Saunderson, *J. Appl. Phys.* **41**, 1433 (1970).
22. J. P. Hodych, *Nature (London)* **298**, 542 (1982).
23. We thank L. Taras Bryndzia for invaluable assistance with the hydrothermal method; G. C. Weatherly for help with the TEM work; D. H. Gorman for donating the magnetite octahedra from Chester, Vermont; R. I. Gait for the magnetite crystals from Nordmarken, Sweden (ROM M11746); M. F. Collins for discussions about inelastic scattering of neutrons by spin-waves; and M. Fuller, P. W. Layer, and H.-U. Worm for comments on the manuscript. The research was supported by Natural Sciences and Engineering Research Council of Canada operating grant A7709 to D.J.D. F.H. thanks the World University Service of Canada for a Government of Canada Award.

22 January 1987; accepted 16 April 1987

Expression of Functional Cell-Cell Channels from Cloned Rat Liver Gap Junction Complementary DNA

G. Dahl,* T. Miller, D. Paul, R. Voellmy, R. Werner

An oocyte expression system was used to test the relation between a complementary DNA (cDNA) clone encoding the liver gap junction protein and cell-cell channels. Total liver polyadenylated messenger RNA injected into oocytes induced cell-cell channels between paired oocytes. This induction was blocked by simultaneous injection of antisense RNA transcribed from the gap junction cDNA. Messenger RNA selected by hybridization to the cDNA clone and translated in oocyte pairs yielded a higher junctional conductance than unselected liver messenger RNA. Cell-cell channels between oocytes were also formed when the cloned cDNA was expressed under the control of a heat-shock promoter. A concentration-dependent induction of channels was observed in response to injection with in vitro transcribed gap junction messenger RNA. Thus, the liver gap junction cDNA encodes a protein that is essential for the formation of functional cell-cell channels.

IT IS GENERALLY ASSUMED THAT GAP junctions represent assemblies of cell-cell channels. This is based on several lines of circumstantial evidence such as the correlation between the presence of gap junctions and intercellular communication (*1, 2*). Over the past 15 years, procedures for isolating gap junctions have been developed that allowed an analysis of their protein components. Molecular sizes for the major gap junction protein ranging from 18,000 to 54,000 daltons have been reported (*3–8*). In part, this wide range of observed molecular sizes may be due to the fact that the gap junctions were obtained from a variety of tissues. However, there is a consensus that the major component of the liver gap junction is a 28,000-dalton protein [but see (*8*)].

It is not known whether the 28,000-dalton protein from liver gap junctions is an essential component of the cell-cell channel, and, if so, whether it can be used to form a functional channel. Two recent developments make it possible to address these questions directly. First, a complementary DNA (cDNA) clone specific for the rat liver gap junction protein has been isolated (*9*). Second, a functional assay for testing channel-specific messenger RNA (mRNA) is now available (*10, 11*). We therefore used the *Xenopus* oocyte cell-cell channel assay in combination with the cDNA clone to examine (i) hybrid arrest of channel formation induced by liver mRNA with antisense RNA, (ii) enrichment of channel-inducing mRNA from rat liver by hybrid selection with gap junction cDNA, (iii) expression of the cloned cDNA under the control of a heat-shock promoter, and (iv) in vitro synthesis of gap junction mRNA from the cloned cDNA and its expression in oocytes.

To test whether the cloned cDNA encodes a critical component of functional cell-cell channels, we used the hybrid-arrest technique (*12–14*). In these experiments antisense RNA specific for the gap junction protein was added to a preparation of total polyadenylated mRNA that is capable of inducing cell-cell channels when injected into oocytes. The induction of such channels in oocytes should be abolished if the cDNA clone, from which the antisense RNA was transcribed, corresponds to the channel gene. To avoid potential problems that could arise from insufficient homology between transcripts in different tissues, we used total polyadenylated mRNA from liver instead of from uterus (*11*) for this experiment. Messenger RNA isolated from rat liver induced a junctional conductance in paired oocytes (Fig. 1 and Table 1). The induction can be seen above a low background (undetectable in several experiments) of endogenous oocyte channels, and the degree of induction is comparable to that observed with uterus or heart mRNA (*15*). Channel induction by liver mRNA was blocked by simultaneous injection of antisense RNA synthesized in vitro from the gap junction cDNA clone. The level of endogenous cell-cell channels, however, was not significantly affected by injection of antisense RNA (Table 1). The observed inhibition of channel formation indicates that an mRNA species that is homologous to, if not identical to, the cloned cDNA is essential for the observed channel induction.

To corroborate these results we used the cloned cDNA to enrich homologous liver mRNA by hybrid selection (*16*). Such hybrid-selected liver mRNA induced channels with higher efficiency than did total mRNA (Table 1), even though the concentration of the selected mRNA was lower than that of polyadenylated total mRNA. In addition, partial degradation probably had occurred. Thus, the cDNA clone can be used to enrich a channel-specific mRNA species from total liver polyadenylated mRNA.

Both hybrid selection and hybrid arrest can be accomplished with incomplete cDNA sequences. Therefore, if the cDNA clone unexpectedly, should not contain the entire sequence, it should still be usable for these experiments. In the next series of experiments, we tested whether the cDNA clone itself can be functionally expressed in oocytes. First, the cDNA sequence, shortened by 500 bases in the 3′-nontranslated region was linked to the promoter of a human heat-shock gene (Fig. 2). Transcription of this construct in heat-treated oocytes was dem-

---

G. Dahl, Department of Physiology and Biophysics, University of Miami School of Medicine, Miami, FL 33101.
T. Miller, R. Voellmy, R. Werner, Department of Biochemistry, University of Miami School of Medicine, Miami, FL 33101.
D. Paul, Department of Anatomy and Cellular Biology, Harvard Medical School, Boston, MA 02115.

*To whom correspondence should be addressed.